Available online at www.sciencedirect.com
ScienceDirect
Solar Energy 81 (2007) 958–968
SOLAR ENERGY
www.elsevier.com/locate/solener

Determination of design space and optimization of solar water heating systems

Govind N. Kulkarni, Shireesh B. Kedare, Santanu Bandyopadhyay *

Energy Systems Engineering, Indian Institute of Technology, Bombay, Powai, Mumbai 400 076, India

Received 11 April 2006; received in revised form 1 December 2006; accepted 12 December 2006
Available online 18 January 2007

Communicated by: Associate Editor Volker Wittwer

Abstract

In this paper, a methodology is proposed to determine the design space for synthesis, analysis, and optimization of solar water heating systems. The proposed methodology incorporates different design constraints to identify all possible designs or a design space on a collector area vs. storage volume diagram. The design space is represented by tracing constant solar fraction lines on a collector area vs. storage volume diagram. It has been observed that there exists a minimum as well as a maximum storage volume for a given solar fraction and collector area. Similarly existence of a minimum and a maximum collector area is also observed for a fixed solar fraction and storage volume. For multi-objective optimization, a Pareto optimal region is also identified. Based on the identified design space, the solar water heating system is optimized by minimizing annual life cycle cost. Due to uncertainty in solar insolation, system parameters and cost data, global optimization may not be utilized to represent a meaningful design. To overcome this, a region of possible design configurations is also identified in this paper.

Keywords: Solar hot water system; Design space; Optimization; Pareto optimal region; Optimal design region

1. Introduction

Proper design of solar water heating system is important to assure maximum benefit to the user, especially for a large system. Designing a solar hot water system involves appropriate sizing of different components based on predicted solar insolation and hot water demand. A number of design methods for solar water heating systems have been proposed in the literature. These methods can be broadly classified into two categories, namely, correlation based methods and simulation based methods. Methods based on utilizability (Duffie and Beckman, 1991), F chart (Klein et al., 1976), $\bar{\phi}$–F chart (Klein and Beckman, 1979), etc. are prominent examples of correlation based methods. Different simulation programs such as TRNSYS (Klein et al., 1975), SOLCHIPS (Lund, 1989; Lund and Peltola, 1992), etc. have been used to design solar hot water systems through detailed simulation approach.

Application of utilizability method for solar hot water systems (Gordon and Rabl, 1982; Pareira et al., 1984) depends on determination of constant critical radiation intensity (Duffie and Beckman, 1991). Application of F charts (Barley and Winn, 1978; Buckles and Klein, 1980; Zeid and Hawas, 1983) assumes a fixed collector loss and an average daily solar irradiation. Applicability of $\bar{\phi}$–F chart method (Braun et al., 1983; Colle and Vidal, 2004) is restricted due to the complexity involved in the calculation of utilizability. Detailed simulation models have been applied for design and optimization of solar hot water systems (Braun et al., 1981; Chang and Minardi, 1980; Ghoneim et al., 1993; Shariah and Lof, 1996; Michaelides and Wilson, 1996; Abdel and Mohamad, 2001; Krause

* Corresponding author. Tel.: +91 22 25767894; fax: +91 22 25726875.
E-mail address: santanu@me.iitb.ac.in (S. Bandyopadhyay).

0038-092X/$ - see front matter © 2006 Elsevier Ltd. All rights reserved.
doi:10.1016/j.solener.2006.12.003

Nomenclature

A_c	collector area, m^2
A_{st}	surface area of the storage tank, m^2
C_c	collector cost coefficient including accessories and piping, US$/$m^2$
C_{OM}	system annual operation and maintenance cost, US$/y
C_F	fuel price, US$/kg
C_p	specific heat of working fluid, J/kg °C
C_R	cost function of domestic LPG water heaters, US$/W
C_{st}	storage system cost coefficient including piping and insulation, US$/$m^2$
CRF_c	capital recovery factor of collector and storage systems, y^{-1}
CRF_{aux}	capital recovery factor of auxiliary heater, y^{-1}
$(CV)_F$	calorific value of fuel, J/kg
F_R	collector heat removal factor
F	solar fraction over a specified time horizon
h/d	height to diameter ratio of storage tank
I_g	global solar radiation intensity, W/m^2
I_d	diffuse radiation intensity, W/m^2
I_T	solar radiation intensity on tilted surface, W/m^2
k	thermal conductivity of storage tank insulation, W/m K
$\dot{m}_L$	desired load mass flow rate, kg/s
$\dot{m}_R$	makeup water mass flow rate, kg/s
$\dot{m}_s$	mass flow rate from storage, kg/s
n	expected life of collectors and storage, y
n_{aux}	expected life of auxiliary heater, y
q_{aux}	rate of auxiliary energy required, W
Q_{aux}	auxiliary energy required over a specified time horizon, J
q_L	rate of desired hot water load, W
Q_L	desired hot water load over a specified time horizon, J
q_{Ls}	load met by solar energy, W
Q_{Ls}	load met by solar energy over a specified time horizon, J
q_s	solar useful heat gain rate, W
Q_s	solar useful heat gain over a specified time horizon, J
q_{stl}	rate of storage loss, W
R	maximum auxiliary heater power, W
R_b	tilt factor
r	discount rate, %
TAC	total annualized system cost, US$
T_a	ambient temperature, °C
T_L	desired load (hot water) temperature, °C
T_R	make up water temperature, °C
T_{sat}	saturation temperature, °C
T_{st}	storage temperature at any instant of time, °C
T_{sti}	storage temperature at the beginning of the time step, °C
T_{stf}	storage temperature at the end of the time step, °C
t	time step in the analysis, s
t_{ins}	storage tank insulation thickness, m
$t_{ins\text{-}av}$	insulation sheet thickness available, m
t_t	storage tank wall thickness, m
U_{st}	storage heat loss coefficient, W/m^2 °C
U_L	collector overall heat loss coefficient, W/m^2 °C
V_{st}	storage volume, m^3

Greek symbols

β	collector tilt, °
ϕ	latitude of location, °
$\bar{\phi}$	solar radiation utilizability
η_{aux}	efficiency of auxiliary heater
η_c	average collector efficiency over a specified time horizon
η_{st}	average storage efficiency over a specified time horizon
ρ	density of working fluid, kg/m^3
ρ_g	ground reflectance
ρ_t	density of storage tank material, kg/m^3
$(\tau\alpha)$	average transmittance absorptance product

Abbreviations

ALCC	annualized life cycle cost
ISO	international standards organization
LPG	liquefied petroleum gas
LPD	liters per day
US$	United States dollar

et al., 2002; Bojic et al., 2002; Mills and Morrison, 2003; Kalogirou, 2004; Chow et al., 2006). Different linear/non-linear optimization techniques (Michelson, 1982; Matrawy and Farkas, 1997) and evolutionary search algorithms (Panteliou et al., 1996; Loomans and Visser, 2002; Kalogirou, 2004) have also been applied. However, development, simulation, validation, and optimization of detailed mathematical model require significant time and effort.

For a given type of solar collector-storage system, parameters such as total collector area, storage volume and solar fraction are important from the performance and optimization point of view. Existing methods identify a single design through optimizing an objective function, such as total annual cost, annualized life cycle cost (Hawlader et al., 1987), life cycle savings (Gordon and Rabl, 1982), pay back period (Michelson, 1982), internal rate of return (Gordon and Rabl, 1982), etc. Therefore, the design of the system depends on the choice of a particular objective function. However, design of a practical solar hot water system is actually a multi-objective task.

It is necessary to determine the entire range of feasible designs possible subject to the availability of solar insolation and demand of hot water. Kulkarni et al. (2006) has introduced a concept of design space to identify all possible and feasible designs of solar hot water systems. The design space is represented on a collector area vs. storage volume diagram, incorporating various design constraints. The proposed methodology (Kulkarni et al., 2006) identifies the design space of solar water heating system with a unity solar fraction ($F = 1$). In this paper, the concept of design space has been extended for different values of solar fraction and the usefulness of design space has been identified for designing solar hot water systems (both grassroots and retrofits). From the set of possible designs, identified through a design space, system designers, manufacturers, and users may choose a particular design considering different objective functions.

2. Mathematical model

Schematic diagram of a solar water heating system is shown in Fig. 1. A typical solar water heating system consists of a solar collector array connected to an insulated storage tank. Solar energy incident on the collectors is carried to the storage tank by circulating water through the collector tubes. The storage meets thermal demand of the load by supplying hot water. Cold makeup water is supplied to the tank as soon as hot water from the tank is withdrawn to meet the load requirement. This arrangement ensures that the storage tank is always full. An auxiliary heater with a bypass is placed in series with the storage in load supply line (Fig. 1) to meet temperature requirement of the load.

Storage tank temperature (T_{st}) is an important parameter which influences the system size and performance. Energy balance of a well mixed storage tank can be expressed as

$$(\rho C_p V_{st})\frac{dT_{st}}{dt} = q_s - q_{Ls} - q_{stl} \tag{1}$$

where the rate of storage loss (q_{stl}) is estimated to be

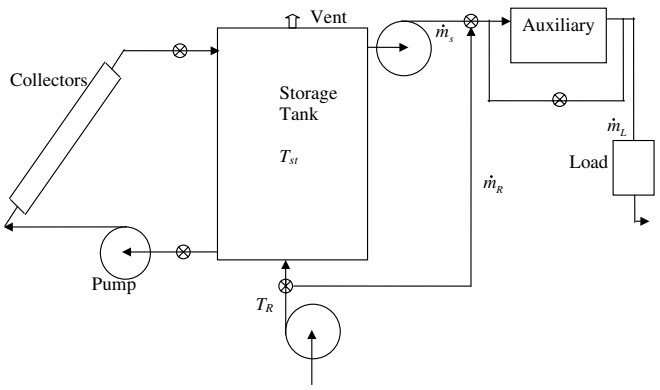

Fig. 1. Schematic of a solar water heating system.

$$q_{stl} = U_{st}A_{st}\cdot(T_{st} - T_a) \tag{2}$$

Solar useful heat gain rate (q_s) from the collector array is calculated (Duffie and Beckman, 1991) as,

$$q_s = A_c[I_T F_R(\tau\alpha) - F_R U_L(T_{st} - T_a)]^+ \tag{3}$$

where + sign indicates that only positive values of q_s to be considered in the analysis. This implies that hot water from the collector enters the tank only when solar useful heat gain becomes positive. Solar flux incident on tilted surface (I_T) is calculated using the following equation.

$$I_T = (I_g - I_d)R_b + I_d\left(\frac{1+\cos\beta}{2}\right) + I_g\left(\frac{1-\cos\beta}{2}\right)\rho_g \tag{4}$$

Combining Eqs. (2) and (3) with Eq. (1), energy balance equation of the tank can be expressed as

$$(\rho C_p V_{st})\frac{dT_{st}}{dt} = A_c[I_T F_R(\tau\alpha) - F_R U_L(T_{st} - T_a)]^+ - q_{Ls} - U_{st}A_{st}\cdot(T_{st} - T_a) \tag{5}$$

During demand, if storage temperature is greater than the desired load temperature ($T_{st} > T_L$), water from the storage tank will be discharged at a rate ($\dot{m}_s$) such that when mixed with appropriate cold makeup water it produces a mixture with desired load temperature (T_L) and flow rate ($\dot{m}_L$). Storage discharge flow rate ($\dot{m}_s$) and make up water flow rate ($\dot{m}_R$) are calculated by considering mass and energy balance at the mixing junction, as

$$\dot{m}_s = \dot{m}_L\frac{T_L - T_R}{T_{st} - T_R} \tag{6}$$

$$\dot{m}_R = \dot{m}_L\frac{T_{st} - T_L}{T_{st} - T_R} \tag{7}$$

Therefore, demand met by solar energy (as long as $T_{st} > T_L$) can be expressed as,

$$q_{Ls} = \dot{m}_s\cdot C_p(T_{st} - T_R) = \dot{m}_L\cdot C_p(T_L - T_R) \tag{8}$$

Whenever during demand, the storage temperature is less than or equal to the desired load temperature ($T_{st} \leqslant T_L$), hot water from the storage is discharged at a rate equal to that of the load ($\dot{m}_s = \dot{m}_L$). In such a case, demand met by the solar energy is determined as,

$$q_{Ls} = \dot{m}_L\cdot C_p(T_{st} - T_R) \tag{9}$$

If $T_{st} < T_L$, the desired load temperature requirement can be met by an auxiliary heater. The duty of auxiliary heater is given by the following formula.

$$q_{aux} = \dot{m}_L\cdot C_p(T_L - T_{st}) \tag{10}$$

Solution of the differential Eq. (5) may be obtained analytically over a time step t, assuming solar radiation intensity on tilted surface (I_T), ambient temperature (T_a), and load demand (q_{Ls}) to be constant over the specified time step. Four different cases have been considered. Analytical solution for the storage temperature (T_{st}) as a function of time (t) for different cases are obtained based on the energy balance equation of the storage tank (5).

Case (i): $T_{st} > T_L$ and $q_s > 0$

$$\frac{[A_c I_T F_R(\tau\alpha) - A_c F_R U_L(T_{stf} - T_a) - \dot{m}_L C_p(T_L - T_R) - U_{st}A_{st}(T_{stf} - T_a)]}{[A_c I_T F_R(\tau\alpha) - A_c F_R U_L(T_{sti} - T_a) - \dot{m}_L C_p(T_L - T_R) - U_{st}A_{st}(T_{sti} - T_a)]} = \exp\left(-\frac{(A_c F_R U_L + U_{st}A_{st})t}{(\rho C_p V_{st})}\right) \quad (11a)$$

Case (ii): $T_{st} > T_L$ and $q_s \leqslant 0$

$$\frac{[-\dot{m}_L C_p(T_L - T_R) - U_{st}A_{st}(T_{stf} - T_a)]}{[-\dot{m}_L C_p(T_L - T_R) - U_{st}A_{st}(T_{sti} - T_a)]} = \exp\left(-\frac{(U_{st}A_{st})t}{(\rho C_p V_{st})}\right) \quad (11b)$$

Case (iii): $T_{st} \leqslant T_L$ and $q_s > 0$

$$\frac{[A_c I_T F_R(\tau\alpha) - A_c F_R U_L(T_{stf} - T_a) - \dot{m}_L C_p(T_{stf} - T_R) - U_{st}A_{st}(T_{stf} - T_a)]}{[A_c I_T F_R(\tau\alpha) - A_c F_R U_L(T_{sti} - T_a) - \dot{m}_L C_p(T_{sti} - T_R) - U_{st}A_{st}(T_{sti} - T_a)]} = \exp\left(-\frac{(A_c F_R U_L + U_{st}A_{st} + \dot{m}_L C_p)t}{(\rho C_p V_{st})}\right) \quad (11c)$$

Case (iv): $T_{st} \leqslant T_L$ and $q_s \leqslant 0$

$$\frac{[-\dot{m}_L C_p(T_{stf} - T_R) - U_{st}A_{st}(T_{stf} - T_a)]}{[-\dot{m}_L C_p(T_{sti} - T_R) - U_{st}A_{st}(T_{sti} - T_a)]} = \exp\left(-\frac{(U_{st}A_{st} + \dot{m}_L C_p)t}{(\rho C_p V_{st})}\right) \quad (11d)$$

It may be noted that whenever the storage temperature (T_{st}) is greater than the desired load temperature (T_L), the load demand is maintained constant by proportionately varying the discharge mass flow rate from the storage tank (8). On the other hand, whenever the storage temperature falls below the desired load temperature ($T_{st} \leqslant T_L$), the maximum possible portions of the demand is met by keeping the discharge mass flow rate equals to the desired load flow rate (10) and rest of the energy demand is met by the auxiliary.

For brevity, demand met by solar energy (q_{Ls}) is assumed to be constant over a time step t and it is calculated based on the initial temperature of the storage tank (T_{sti}). The error introduced due to this simplification may be reduced by taking smaller time step.

For a cylindrical tank, the surface area of the tank is related to the storage volume of the tank by the following equation:

$$A_{st} = 1.845(2 + h/d)V_{st}^{2/3} \quad (12)$$

Similar expression for other type of storage tanks can also be derived.

For a given type of collector (i.e., with given $F_R U_L$ and $F_R(\tau\alpha)$), storage tank loss coefficient (U_{st}), insolation on the tilted surface (I_T) and the thermal load characteristics ($\dot{m}_L$ and T_L), Eq. (11) uniquely predicts the temperature profile inside the storage tank as a function of collector area (A_c) and storage volume (V_{st}).

A time horizon may be specified for the analysis. A time horizon may be a day, a month or a year depending on the period of interest. Total desired load, contribution of the solar energy towards the total load, and the total auxiliary energy requirement over a specified time horizon may be expressed as follows:

$$Q_L = \sum \int_0^t \dot{m}_L \cdot C_p(T_L - T_R)\,dt \quad (13)$$

$$Q_{Ls} = \sum \int_0^t \dot{m}_s \cdot C_p(T_{st} - T_R)\,dt \quad (14)$$

$$Q_{aux} = Q_L - Q_{Ls} = \sum_t \int_0^t [\dot{m}_L \cdot C_p(T_L - T_R) - \dot{m}_s \cdot C_p(T_{st} - T_R)]^+\,dt \quad (15)$$

The + sign in Eq. (15) indicates that only positive values of auxiliary are to be accounted for. The solar fraction over the time horizon may be calculated as:

$$F = \frac{Q_{Ls}}{Q_L} = 1 - \frac{Q_{aux}}{Q_L} \quad (16)$$

Average collector and storage efficiencies may be defined as follows:

$$\eta_c = \frac{\sum \int_0^t [I_T F_R(\tau\alpha) - F_R U_L(T_{st} - T_a)]^+\,dt}{\sum \int_0^t I_T\,dt} \quad (17)$$

$$\eta_{st} = \frac{\sum \int_0^t U_{st}A_{st}(T_{st} - T_a)\,dt}{1 - \sum \int_0^t [I_T F_R(\tau\alpha) - F_R U_L(T_{st} - T_a)]^+\,dt} \quad (18)$$

Generation of design space is introduced in the next section. For simplicity and clarity, analysis of a single day has been presented through an example. More generalized design space considering annual performance of the systems with different solar fractions will be discussed later in the paper.

3. Generation of design space

The methodology of design space generation is illustrated through an example of domestic hot water system. The various system parameters for this example are given in Table 1. Monthly mean values of hourly solar radiation

Table 1
System parameters and input data for domestic hot water example

Location	Apartment building at Pune (18.53° North, 73.85° East), India
Load	Domestic hot water load, 4500 LPD at 60 °C Consumption pattern as per ISO 9459–3:1997(E). The profile is shown in Fig. 2 (International Standards Organization, 1997)
Collectors	Flat plate collectors (single cover and selective coated) $F_R(\tau\alpha) = 0.675$ and $F_R U_L = 5.656$ W/m^2 K South facing with tilt of 33.5° Ground reflectance, $\rho_g = 0.2$
Storage	Cylindrical, well mixed, always full, with $(h/d) = 1$ Mild steel, wall thickness 6 mm, density 7800 kg/m^3 Insulation: glass wool ($k = 0.04$ W/m K) and 0.2 m thick

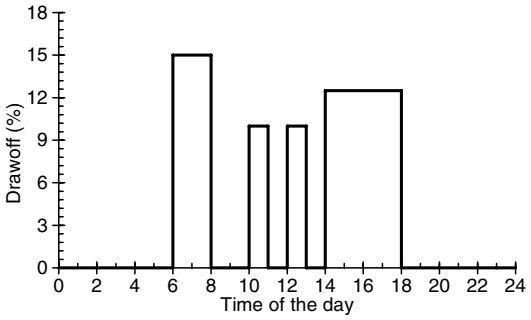

Fig. 2. Domestic hot water consumption pattern as per ISO 9459-3:1997 (ISO, 1997).

(Mani, 1981) on April 15 are used for this example. The parameters are consistent with to the configuration shown in Fig. 1. In this example, the load temperature is 60 °C and the draw off profile of the load is shown in Fig. 2. In this example, of one day analysis, time step t is taken as 5 min (300 s). The system parameters are used to solve the mathematical model over a 24 h time horizon.

Solution of the mathematical model calls for specified collector area (A_c), storage volume (V_{st}), and initial storage temperature estimate. At the start, storage temperature is assumed to be ambient i.e. 25 °C. With a collector area of 80 m^2 and a storage volume of 5 m^3, storage temperature is observed to be 55.11 °C at the end of the day. Assuming this as the starting temperature for next day, final temperature of the next day may be calculated. Fig. 3 shows variation of storage temperatures at the beginning and at the end of a day (time horizon) for number of successive days. The difference between temperatures at the beginning and at the end of the day decreases with number of cycles (days). It may be observed from Fig. 3 that on the seventh day the storage temperature at the beginning and at the end of the day is almost same (69.52 °C). It may be concluded that the storage temperature profile attains equilibrium in about 6 cyclic operations. It may be noted that the equilibrium of storage temperature profile does not imply that the temperature is constant all over the day. It only suggests that the temperature profile (including its variation over the day) does not change day by day. In a sense, it reaches a steady-state. For proper design of the system, transient behavior of temperature profile is neglected in this paper.

In this paper, it is assumed that the temperature profile reaches a steady state condition. This implies that the net gain or loss of the stored thermal energy for the storage tank over a given time horizon of analysis is zero.

$$\sum \int_0^t \left(\rho C_p V_{st} \frac{dT_{st}}{dt} \right) dt = 0 \tag{19}$$

3.1. Limits on storage temperature profile

By varying collector area and storage volume, different designs may be obtained. Steady state storage temperature profile for the example is shown in Fig. 4 for a collector area of 90 m^2 and a storage volume of 12 m^3. Initially, it is assumed to supply complete thermal load ($F = 1$), the temperature of the storage tank during load has to be greater than the desired load temperature.

$$T_{st} \geqslant T_L \tag{20}$$

For this example the load temperature is 60 °C. Therefore, for any acceptable design with unity solar fraction, the storage temperature has to be greater than 60 °C during load.

In this example, of solar water heating system, water is used as a working fluid. The system cannot be designed for two-phase condition. The storage tank temperature, therefore, has to be always less than the boiling temperature of working fluid.

$$T_{st} \leqslant T_{sat} (=100\ ^\circ C) \tag{21}$$

An acceptable design must satisfy the above two constraints stated by Eqs. (20) and (21). For the specified load, all possible combinations of collector area and storage volume that satisfy these two constraints define the design space. It may be identified on a collector area vs. storage volume diagram.

3.2. Establishment of design limit based on load temperature

A combination of collector area (A_c) and storage volume (V_{st}) that satisfies the load temperature criterion as defined in Eq. (20) establishes the design limit. For the first example, Fig. 5 illustrates this design limit. For a given collector area, a maximum and a minimum storage volume

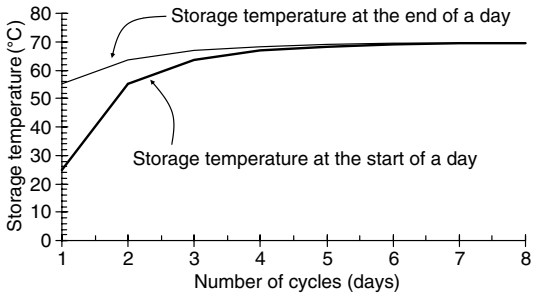

Fig. 3. Variation of storage temperature at the start and at the end of a day over number of cycles (days).

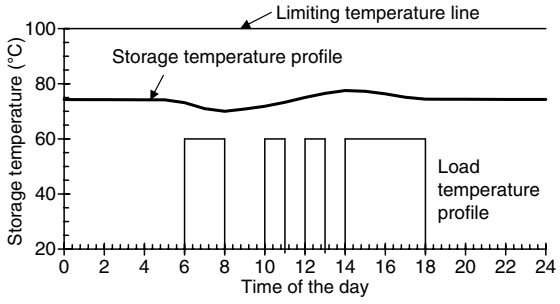

Fig. 4. Storage temperature profile over a typical day for ISO load with a system size of $A_c = 90\ m^2$ and $V_{st} = 12\ m^3$.

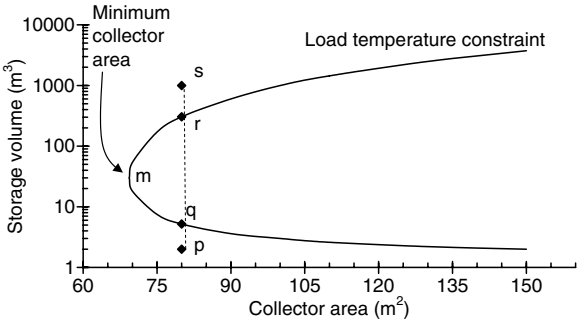

Fig. 5. Establishment of design limit based on load temperature on a collector area vs. storage volume diagram.

are searched to produce a temperature profile that satisfies Eq. (20). As an illustration, it is demonstrated in Fig. 5 that a design size corresponding to a collector area of 80 m^2, a volume of 5.2 m^3 and a volume of 305 m^3 produce a temperature profile that satisfies Eq. (20). These are denoted as points 'q' and 'r' in Fig. 5. Steady-state temperature profiles correspond to these conditions are shown in Fig. 6a and b. Any volume in between these limits also produces a temperature profile that satisfies load temperature requirement. In this figure, point 'p' exhibits a non-feasible system configuration ($A_c = 80$ m^2 and $V_{st} = 2$ m^3) for unity solar fraction ($F = 1$). Temperature profile corresponding to this configuration ($A_c = 80$ m^2 and $V_{st} = 2$ m^3) is shown in Fig. 6c. It may be observed that the storage temperature drops below 60 °C during load. Similarly, increase in the storage volume beyond 305 m^3 produces an infeasible system configuration. To illustrate, a system configuration ($A_c = 80$ m^2 and $V_{st} = 1000$ m^3) represented by point 's' in Fig. 5 has been considered. Temperature profile corresponding to this configuration is shown in Fig. 6d.

Similar exercise is performed for different collector area to identify the design limit based on load temperature, as illustrated in Fig. 5.

It may be observed that reduction in collector area reduces the difference between the maximum and the minimum values of storage volume. At the limit (point 'm' in Fig. 5), there exists no difference between the upper and the lower bound on storage volume. This point signifies the minimum collector area requirement and corresponds to a unique storage volume required for this example. Any further reduction in collector area will fail to satisfy the load temperature requirement. Temperature profile (not shown for brevity) of the storage tank will be equivalent to Fig. 6a.

Existence of a maximum and a minimum storage volumes for a given collector area to satisfy the load temperature requirement may be understood in the following way. In the proposed configuration, storage volume is equivalent to a thermal capacitor. Therefore, increase in storage volume reduces the fluctuations in storage temperatures over a day. As the storage volume increases, inlet temperature to the collector array decreases and thereby increases the average collector efficiency (17). However,

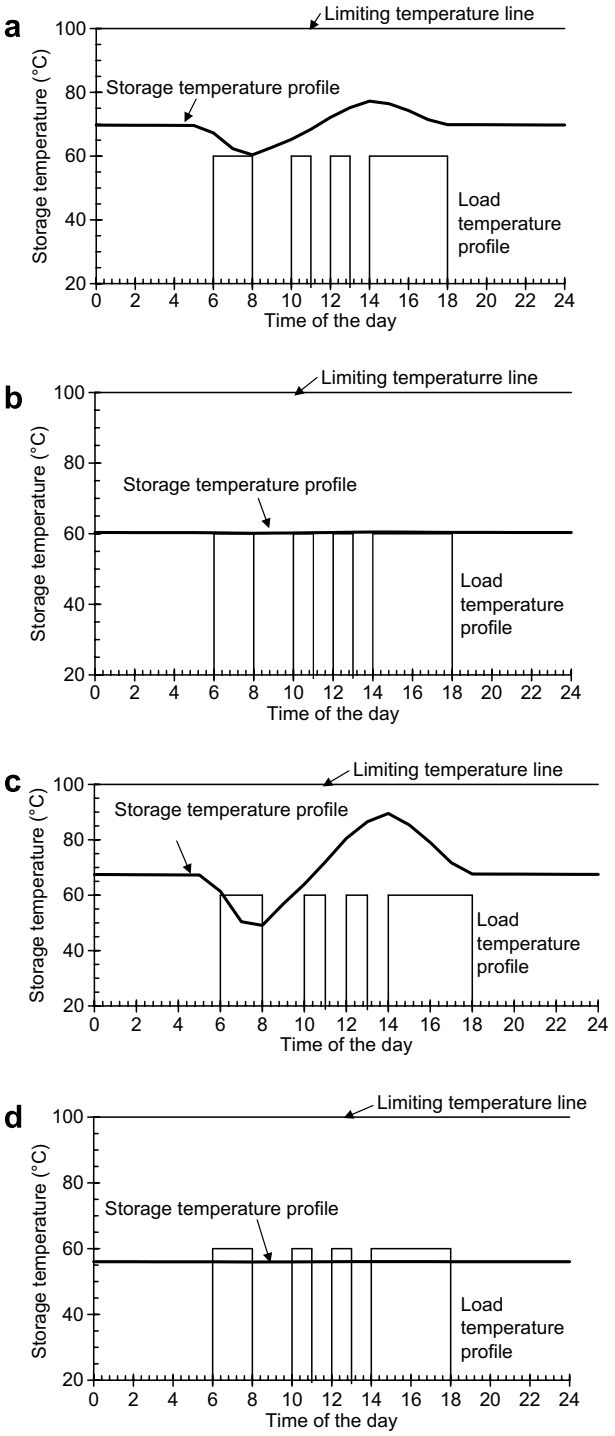

Fig. 6. Storage temperature profile for different systems configurations: (a) a feasible design case for $F = 1$ for a system configuration of $A_c = 80$ m^2 and $V_{st} = 5.2$ m^3; (b) a feasible design case for $F = 1$ for a system configuration of $A_c = 80$ m^2 and $V_{st} = 305$ m^3; (c) an infeasible design case for a system configuration of $A_c = 80$ m^2 and $V_{st} = 2$ m^3, and (d) an infeasible design case for a system configuration of $A_c = 80$ m^2 and $V_{st} = 1000$ m^3.

increase in storage volume increases the storage surface area (12) and thereby increases the storage losses (2). Hence, increase in storage volume reduces the average storage efficiency (18). Variations in average collector and

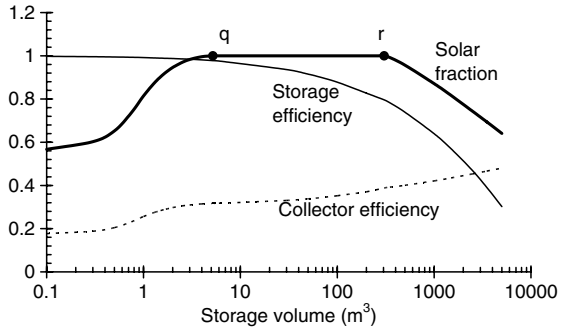

Fig. 7. Effect of storage volume on storage efficiency, collector efficiency, and solar fraction ($A_c = 80\ m^2$).

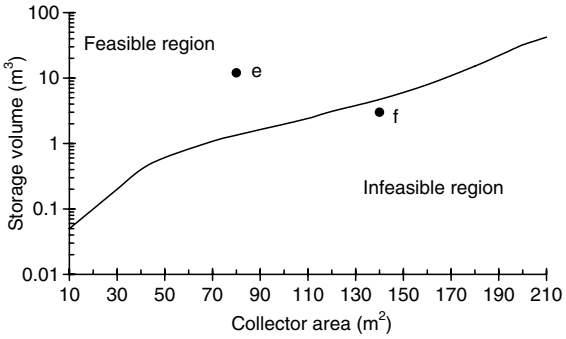

Fig. 8. Establishment of design limit based on maximum fluid temperature.

storage efficiencies with storage volume for a collector area of 80 m^2 are shown in Fig. 7. Change in solar fraction with storage volume is also shown in Fig. 7.

It may be observed that for low storage volumes, the rate of decrease of average storage efficiency is nominal and the rate of increase in average collector efficiency is high. This implies that the increase in storage volume in this regime increases storage temperature and improves solar fraction (Fig. 7). It reaches a maximum of unity as highlighted by point 'q' in Fig. 7. It remains constant till point 'r' in the same figure. After point 'r', the solar fraction reduces with increasing storage volume. In the regime of very high storage volume, it may be observed that the rate of decrease of average storage efficiency is significant compared to the rate of increase in average collector efficiency. This implies that the increase in storage volume in this regime reduces solar fraction from unity (Fig. 7).

3.3. Establishment of design limit based on maximum temperature

For very low storage volumes, fluctuations in storage temperature are high. Since, water is the working fluid; the maximum temperature of the storage tank is not allowed to increase beyond the temperature at which water starts boiling. This limitation is expressed mathematically in Eq. (21). For a given collector area, minimum volume is determined such that the temperature profile always remains below this maximum allowed temperature limit. Fig. 8 represents this graphically on a collector area vs. storage volume diagram. It essentially divides the entire region into two parts, an infeasible region where temperature profiles go beyond the maximum allowed limit and a feasible region. Point 'e' in Fig. 8 represents a feasible design point. The storage temperature profile for this design configuration ($A_c = 80\ m^2$ and $V_{st} = 12\ m^3$) is shown in Fig. 9a. On the other hand, point 'f' in Fig. 8 represents an infeasible design point. Storage temperature profile corresponding to this point ($A_c = 140\ m^2$ and $V_{st} = 3\ m^3$) is shown in Fig. 9b. It may be observed that the temperature profile for the second point exceeds allowable maximum temperature of 100 °C.

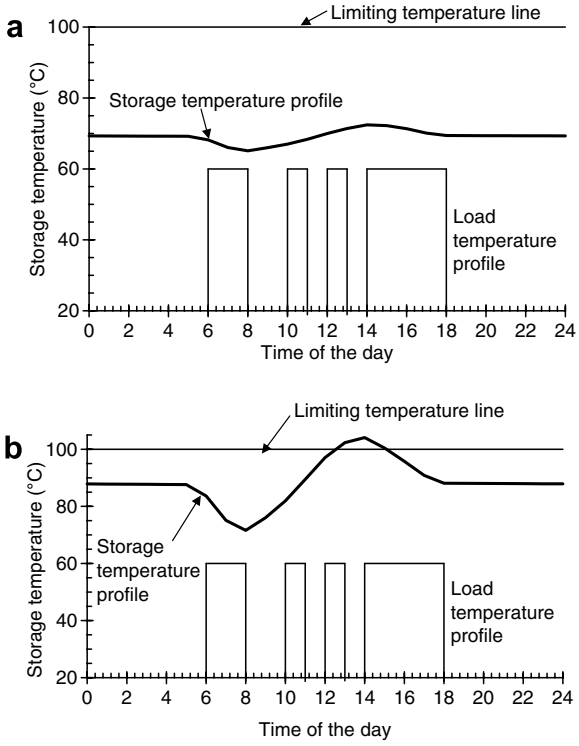

Fig. 9. Storage temperature profile for different systems configurations: (a) a feasible design case for system configuration of $A_c = 80\ m^2$ and $V_{st} = 12\ m^3$ and (b) an infeasible design case for system configuration of $A_c = 140\ m^2$ and $V_{st} = 3\ m^3$.

3.4. Overall design space and its significance

Based on the design limits described in previous sections, a combined feasible design space may be obtained. Fig. 10 shows the overall design space. Any point inside this feasible design space simultaneously satisfies the load temperature requirement (20) and maximum allowed temperature limit (21).

It may be observed that for any given collector area there exist a maximum and a minimum storage volume limits. On the other hand, it may also be observed that for any given storage volume there exist a maximum and a minimum collector area limits.

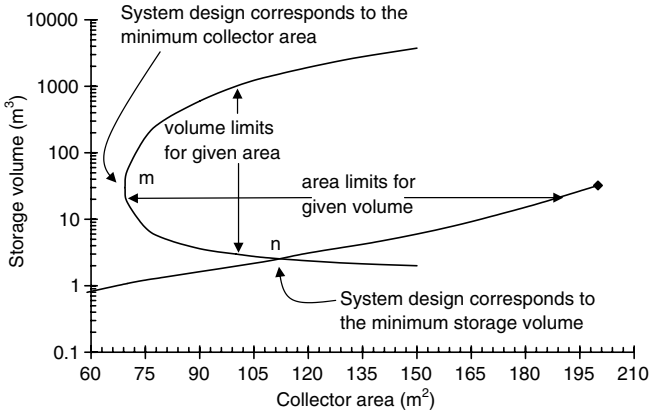

Fig. 10. The complete design space for unity solar fraction.

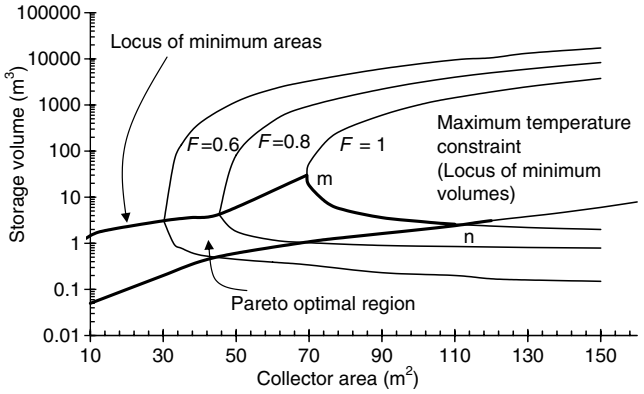

Fig. 12. Design space for different solar fraction with single day analysis and identification of Pareto optimal region.

Another interesting observation may be made on the overall design space. Intersection of the two limiting curves denotes the minimum storage volume (point 'n' in Fig. 10). Therefore, there exists a design configuration ($A_c = 69.4$ m^2 and $V_{st} = 30$ m^3) corresponding to the minimum collector area (point 'm' in Fig. 10) and a design configuration ($A_c = 113$ m^2 and $V_{st} = 2.4$ m^3) corresponding to the minimum storage volume (point 'n' in Fig. 10).

Any objective function considering capital costs of the collector array and that of the storage volume may be chosen for optimization. Depending upon the cost data, a unique solution may be obtained. Since the collector cost increases with the collector area and the storage cost increases with the storage volume, the optimal point lies on the line segment 'm–n' in Fig. 10 of the design space. The line segment 'm–n' signifies the Pareto optimality curve (as highlighted in Fig. 11). Any suitable multi-objective optimization can also be performed to choose an appropriate configuration of the system.

Pareto optimal curve highlights that if the line segment 'm–n' shrinks to a point, then this point represents a unique design configuration and no optimization is required. However, from a practical view point, it is desired to design the system not on the Pareto curve but little inside the feasible curve to incorporate uncertainty in solar insolation.

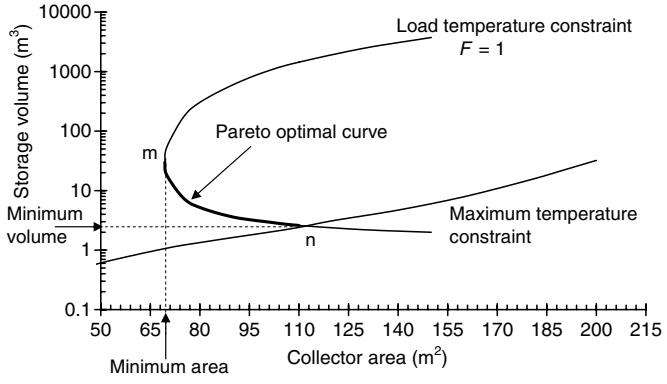

Fig. 11. Identifying Pareto optimal curve on the design space for unity solar fraction.

Extending the design space for different solar fractions is discussed next.

3.5. Design space with different solar fractions

It may be noted that the limiting curve obtained for maximum allowable storage temperature is independent of the specified load temperature. Therefore, for different solar fractions this limiting condition remains the same. However, limiting curve obtained using load temperature constraint changes due to different solar fraction. For a given solar fraction and a given collector area, a maximum and a minimum storage volume may be obtained by solving the model equations. While solving the model equations, Eq. (20) may be relaxed and average solar fraction over the time horizon (16) should be greater than or equal to the predefined solar fraction. Calculating the limiting volumes for different collector areas, a limiting curve corresponds to a predefined solar fraction may be obtained. Fig. 12 shows the limiting curves for different solar fractions. It may be noted that any point inside a limiting curve (for a specified solar fraction) corresponds to a solar fraction that is greater than or equal to the specified value.

The loci of the minimum collector area and minimum storage volume for different solar fractions are also shown in Fig. 12. It may be noted that the area enclosed by these loci and the curve segment 'm–n' for $F = 1$ defines the Pareto optimal region.

Application of the above mentioned methodology to annual case and economic optimization with a particular objective function are demonstrated in the next section.

4. Design space for annual performance and economic optimization

In the previous section, time horizon of a single day was considered. In this section, the time horizon has been extended to a year. The single day model described in Section 2 is extended over an annual basis. The various system parameters remain same as in Table 1. Monthly mean

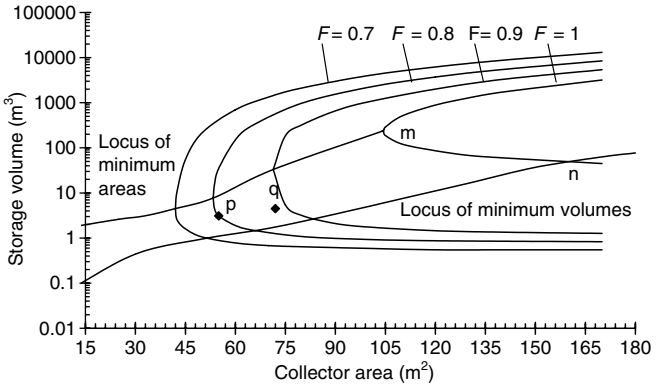

Fig. 13. Design space for annual performance (optimum system size at point 'p' corresponds to $A_c = 55\ m^2$ and $V_{st} = 3.1\ m^3$).

values of hourly solar radiation data are used (Mani, 1981). Each month is modeled as six days to reduce computational complexity.

Applying similar methodology as described in the previous section, limiting curves for the annual performance of the system for different solar fraction are shown in Fig. 13. The loci of the minimum collector area and minimum storage volume for different solar fractions are also shown. Based on the Pareto optimal region, as discussed in the previous section, a multi-objective optimization may be performed to design the system. For brevity, a single economic objective function has been chosen to illustrate optimization procedure.

4.1. Economic optimization and optimal region

To balance the economic benefits of energy savings and capital investment, an economic objective function based on the annualized life cycle cost (ALCC) has been chosen for the analysis. The objective function is formulated as total annual cost (TAC) of the system,

$$\mathrm{TAC} = (C_c A_c + C_{st} A_{st})\mathrm{CRF}_c + C_{OM} + (C_R R)\mathrm{CRF}_{aux} + \frac{(1-F)Q_L \cdot C_F}{(\mathrm{CV})_F \eta_{aux}} \quad (22)$$

The capital recovery factor is calculated based on the following expression.

$$\mathrm{CRF} = \frac{r(1+r)^n}{(1+r)^n - 1} \quad (23)$$

The cost coefficients are based on the existing market trends in India. The cost coefficients for economic optimization are given in Table 2. It may be noted that the cost coefficient for the storage tank is expressed in terms of its surface area. Operating and maintenance cost for the system has been taken as 2% of the capital cost. An auxiliary of LPG fired online heater has been considered in this example. The calorific value of LPG is 50.3 MJ/kg and the burner efficiency is assumed to be 80%. Rating of the auxiliary heater (R) is determined by the maximum duty required over the entire year.

Table 2
Economic parameters adopted for optimization

Discount rate, r%	10.75
Life of collectors and storage, n years	15
Life of auxiliary, n_{aux} years	10
Collector cost coefficient, C_c US$/m^2	106.8
Storage tank cost coefficient, C_{st} US$/m^2	84.2
Tank insulation price, C_{ins} US$/m^2	2.67 (for a slab thickness of 25.4 mm)
Cost coefficient for LPG water heaters, C_R US$/W	0.055
Fuel price, C_F US$/kg	0.47

Note: For currency conversion, it has been considered that 1 US$ = 45.05 Rs. (Reserve Bank of India, 2006).

Variation of the minimum annualized capital cost as a function of solar fraction is shown in Fig. 14. It may be noted that the capital cost increases with increasing solar fraction. As the solar fraction increases, the auxiliary and hence, the operating cost decreases. Variation of operating cost for different solar fraction is also shown in Fig. 14. This implies classical capital-energy trade offs. Variation of annualized life cycle cost for different solar fraction is shown in Fig. 14. The search technique results in an optimum TAC of 1840 US$/y at a solar fraction of $F = 0.8$. Corresponding collector area and storage volume are 55 m^2 and 3.1 m^3, respectively. The optimum design point, obtained by minimizing TAC is indicated as point 'p' in the Pareto optimal region in Fig. 13. It may be mentioned that in India, a typical domestic supplier would supply a 2 m^2 collector area with a 0.125 m^3 tank to deliver 0.125 m^3 of hot water over a day at 60°C. For this example, any commercial supplier would have supplied a system with 72 m^2 of collector area and a storage tank of 4.5 m^3. This is shown as point 'q' in Fig. 13 for ready reference. This configuration corresponds to a TAC of 1920 US$/y. This is 4% higher than the minimum.

It may be noted that the TAC curve in Fig. 14 increases rapidly for higher solar fraction. The steep rise in the system cost is due to steep rise in collector area requirement to meet higher solar fraction. To meet higher solar fraction, average storage temperature has to be increased and increase in storage temperature (which is also the collector inlet temperature) reduces the collector efficiency.

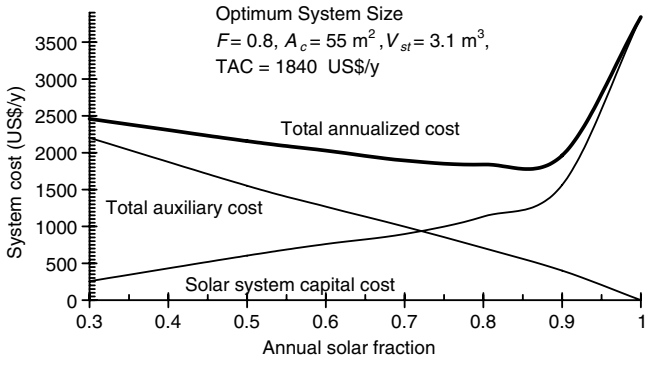

Fig. 14. Determination of optimum solar fraction.

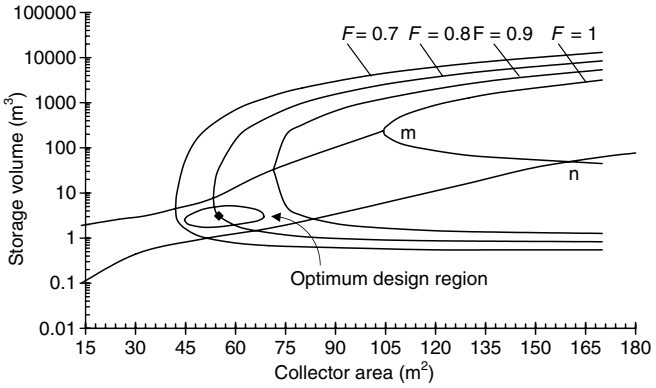

Fig. 15. Identification of optimum design region such that the total annualized cost is within 2% of the minimum value.

From Fig. 14, it may be noted that the TAC curve does not change significantly near the global optimum. Due to uncertainties associated with system parameters, solar insolation, cost data, etc. a globally optimum value may not necessarily provide a meaningful result in actual practice. Similar observations were reported by Shenoy et al. (1998) in designing and optimizing heat exchanger networks. The TAC vs. solar fraction curve is found to be fairly flat in the neighborhood of the minimum TAC. Consequently, it is better to define the optimum solar fraction in terms of a range rather than a single value. A range of solar fraction may be estimated such that the TAC lies within 2% of its minimum value. In this example, the range for solar fraction is estimated to be in between 0.72 and 0.87. At the lower solar fraction ($F = 0.72$) the system configuration ($A_c = 45\ m^2$ and $V_{st} = 2.5\ m^3$) calls for lower capital investment (937 US$/y) and higher auxiliary energy (939 US$/y). On the other hand, higher solar fraction ($F = 0.87$) implies a system configuration ($A_c = 68\ m^2$ and $V_{st} = 3.0\ m^3$) with higher capital investment (1346 US$/y) and lower operating cost (527 US$/y). Based on the available cash flow for investment, designer may choose an appropriate system configuration. All possible design combinations such that the corresponding TAC is within 2% of the minimum value, are identified on the design space (Fig. 15).

5. Conclusions

The concept of design space approach for synthesis, analysis, and optimization of solar thermal system is presented in this paper. Existence of design space is attributed to the specification of demand and limiting storage condition. Design space offers flexibility in system sizing. However, it is specific for a given configuration. Employment of the design space approach for optimization and parametric analysis of solar thermal systems may reduce the labor, expertise, and expense involved. The methodology is simple, flexible and does not need any special computational setup, thus offering a prospect of application in domestic as well as industrial configurations. The proposed methodology helps in clear understanding of the behavior of the system with different storage volumes and collector areas supplying a specified load, thus revealing constraints and flexibilities.

The proposed methodology does not identify a unique system design by optimizing any particular objective function. A range of system designs can easily be identified using the proposed methodology. This offers flexibility for the system designer. As demonstrated through an example, system designer may choose a particular configuration, not necessarily the mathematically optimum one, depending upon the available cash flow for the project implementation. This is especially important for designing industrial systems.

The proposed design space approach may be useful in retrofit cases as well. The method still identifies a range of possible designs with specified collector area or specified storage volume. Constraints such as existing collector area, limitations on available floor spacing, existing storage volume, or maximum allowable storage volume due to structural restriction, etc. can easily be incorporated in the proposed methodology.

For polymeric collectors, the maximum allowed temperature of the water becomes even more important to prevent over heating of the collectors and consequent damages. The proposed methodology can be applied to many different solar thermal configurations. Future research is directed towards the same.

Acknowledgements

Authors express their appreciation to Prof. J.K. Nayak and Prof. R. Banerjee, Energy Systems Engineering, Indian Institute of Technology (IIT), Bombay, for their inputs and insightful comments during various stages of this work.

References

Abdel, A.M., Mohamad, M.A., 2001. Potential of solar energy utilization in the textile industry – a case study. Renewable Energy 23, 685–694.

Barley, C.D., Winn, C.B., 1978. Optimal sizing of solar collectors by the method of relative areas. Solar Energy 21, 279–289.

Bojic, M., Kalogirou, S., Petronijevic, K., 2002. Simulation of solar domestic water heating system using a time marching model. Renewable Energy 27, 441–452.

Braun, J.E., Klein, S.A., Mitchell, J.W., 1981. Seasonal storage of energy in solar heating. Solar Energy 26, 403–411.

Braun, J.E., Klein, S.A., Pearson, K.A., 1983. An improved design method for solar water heating systems. Solar Energy 31, 597–604.

Buckles, W.E., Klein, S.A., 1980. Analysis of solar domestic hot water heaters. Solar Energy 25, 417–424.

Chang, K.K., Minardi, A., 1980. Optimization formulation for solar heating systems. Solar Energy 24, 99–103.

Chow, T.T., Fong, K.F., Chan, A.L.S., Lin, Z., 2006. Potential application of centralized solar water heating system for a high-rise residential building in Hong Kong. Applied Energy 83, 42–54.

Colle, S., Vidal, H., 2004. Upper bounds for thermally driven cooling cycles optimization derived from the $f - \bar{\phi}$ chart method. Solar Energy 76, 125–133.

Duffie, J.A., Beckman, W.A., 1991. Solar Engineering of Thermal Processes, second ed. Wiley, New York, pp. 686–732.

Ghoneim, A.A., Fisch, N., Ammar, A.S.A., Hahne, E., 1993. Design of a solar water heating system for Alexandria, Egypt. Renewable Energy 3, 577–583.

Gordon, J.M., Rabl, A., 1982. Design analysis and optimization of industrial process heat plants without storage. Solar Energy 28, 519–530.

Hawlader, M.N.A., Ng, K.C., Chandratilleke, I.T., Sharma, D., Koay, K.H.L., 1987. Economic evaluation of a solar water heating system. Energy Conversion Management 27, 197–204.

ISO 9459-3:1997(E), 1997. Performance Tests for Solar plus supplementary Systems. International Standards Organization, Geneva, Switzerland, p. 9.

Kalogirou, S.A., 2004. Optimization of solar systems using artificial neural networks and genetic algorithms. Applied Energy 77, 383–405.

Klein, S.A., Beckman, W.A., 1979. A general design method for closed loop solar energy systems. Solar Energy 22, 269–282.

Klein, S.A., Cooper, P.I., Freeman, T.L., Beekman, D.L., Beckman, W.A., Duffie, J.A., 1975. A method of simulation of solar processes and its application. Solar Energy 17, 29–37.

Klein, S.A., Beckman, W.A., Duffie, J.A., 1976. A design procedure for solar heating systems. Solar Energy 18, 113–127.

Krause, M., Vajen, K., Wiese, F., Ackerman, H., 2002. Investigations on optimizing large solar thermal systems. Solar Energy 73, 217–225.

Kulkarni, G.N., Kedare, S.B., Bandyopadhyay, S., 2006. The Concept of Design Space for Sizing Solar Hot Water Systems. In: Sastry, E.V.R., Reddy, D.N. (Eds.), Proceedings of International Congress on Renewable Energy 2006, Hyderabad, India, pp. 302–305.

Loomans, M., Visser, H., 2002. Application of genetic algorithm for optimization of large solar hot water systems. Solar Energy 72, 427–439.

Lund, P.D., 1989. General design methodology for seasonal storage solar systems. Solar Energy 42, 235–251.

Lund, P.D., Peltola, S.S., 1992. SOLCHIPS – A fast pre-design and optimization tool for solar heating with seasonal storage. Solar Energy 48, 291–300.

Mani, A., 1981. Hand Book of Solar Radiation Data for India, first ed. Allied Publishers Pvt. Ltd., New Delhi, pp. 381–397.

Matrawy, K.K., Farkas, I., 1997. New technique for short term storage sizing. Renewable Energy 11, 129–141.

Michaelides, I.M., Wilson, D.R., 1996. Optimum design criteria for solar hot water systems. Renewable Energy 9, 649–652.

Michelson, E., 1982. Multivariate optimization of a solar water heating system using the simplex method. Solar Energy 29, 89–99.

Mills, D., Morrison, G.L., 2003. Optimization of minimum backup solar water heating system. Solar Energy 74, 505–511.

Panteliou, S., Dentsoras, A., Daskalopoulas, E., 1996. Use of expert systems for the selection and the design of solar domestic hot water systems. Solar Energy 57, 1–8.

Pareira, M.C., Gordon, J.M., Rabl, A., Zarmi, Y., 1984. Design and optimization of solar industrial hot water systems with storage. Solar Energy 32, 121–133.

Reserve Bank of India, 2006. <www.rbi.org.in/home.aspx>.

Shariah, A.M., Lof, G.O.G., 1996. Optimization of tank volume-to-collector area ratio for a thermosyphon solar water heater. Renewable Energy 7, 289–300.

Shenoy, U.V., Sinha, A., Bandyopadhyay, S., 1998. Multiple utilities targeting for heat exchanger networks. Trans. IChemE: Chem. Engg. Research. & Design 76 (3), 259–272.

Zeid, M.R.A.A., Hawas, M.M., 1983. Economic evaluation and optimization of solar systems for space and domestic water heating. Solar Energy 23, 251–256.